Philosophical Magazine
Publication details, including instructions for authors and subscription information:
http://www.tandfonline.com/loi/tphm20

Effect of alloying element on dislocation cross-slip in γ'-Ni_3Al: a first-principles study

Xiao-Xiang Yu [a b] & Chong-Yu Wang [b c]

[a] Department of Material Science and Engineering, Tsinghua University, Beijing 100084, China

[b] Department of Physics, Tsinghua University, Beijing 100084, China

[c] The International Centre for Materials Physics, Chinese Academy of Sciences, Shenyang 110016, China

Published online: 10 Jul 2012.

To cite this article: Xiao-Xiang Yu & Chong-Yu Wang (2012) Effect of alloying element on dislocation cross-slip in γ'-Ni_3Al: a first-principles study, Philosophical Magazine, 92:32, 4028-4039, DOI: 10.1080/14786435.2012.700419

To link to this article: http://dx.doi.org/10.1080/14786435.2012.700419

Philosophical Magazine
Vol. 92, No. 32, 11 November 2012, 4028–4039

Effect of alloying element on dislocation cross-slip in γ'-Ni_3Al: a first-principles study

Xiao-Xiang Yu[ab] and Chong-Yu Wang[bc]*

[a]*Department of Material Science and Engineering, Tsinghua University, Beijing 100084, China;* [b]*Department of Physics, Tsinghua University, Beijing 100084, China;* [c]*The International Centre for Materials Physics, Chinese Academy of Sciences, Shenyang 110016, China*

(*Received 2 February 2012; final version received 25 May 2012*)

The effects of alloying elements Re, Ru, Ta, Ti, and W on the activation enthalpy of dislocation cross-slip in γ'-Ni_3Al are studied combining density functional theory calculations with the classical theory of dislocations. The elements Re and W are found to effectively increase planar fault energies on the (111) plane and decrease the cross-slip activation enthalpy in Ni_3Al. The reduction of activation enthalpy will increase the probabilities of cross-slipping and forming sessile dislocation locks. Therefore, Re and W can inhibit the further motion of dislocations and raise the flow stress of Ni_3Al in the anomalous temperature regime. The underlying electronic mechanism is the strong bonding of Re–Ni and W–Ni and the weak bonding of Re–Al and W–Al in fault areas.

Keywords: density functional theory; dislocation mobility; electronic structure; plastic flow properties

1. Introduction

Nickel-based single-crystal superalloys with extraordinary mechanical properties at high temperatures are critical to high-performance aero engines [1,2]. The typical microstructure of these alloys involves the precipitation of the γ'-Ni_3Al phase with $L1_2$ structure coherently embedded in a matrix of the γ-Ni phase. γ'-Ni_3Al, with anomalous temperature dependence of the yield stress, is largely responsible for the strength of superalloys and their resistance to deformation at high temperatures [3]. It is widely accepted that the anomalous flow behavior of Ni_3Al is caused by thermally activated cross-slip of the screw dislocations from the (111) primary slip plane onto the (001) cube plane. The cross-slipped screw dislocations form a Kear–Wilsdorf (KW) lock, thus the glide of the dislocation is restricted [4]. Paidar, Pope and Vitek (PPV) proposed a model giving the details of the pinning mechanism [5], which was modified later by Yoo [6]. A perfect dislocation slipping on the (111) plane in Ni_3Al consists of four Shockley partial dislocations ($P_1 = P_3$ and $P_2 = P_4$) bounding one antiphase boundary (APB) fault and two complex stacking faults (CSF) as shown in Figure 1a [7,8]. After cross-slip, the dislocation lock forms as

*Corresponding author. Email: cywang@mail.tsinghua.edu.cn

ISSN 1478–6435 print/ISSN 1478–6443 online

http://dx.doi.org/10.1080/14786435.2012.700419
http://www.tandfonline.com

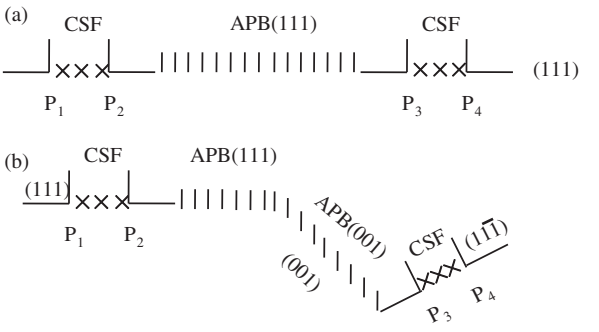

Figure 1. Sketch map of screw dislocation cross-slip in Ni_3Al. (a) Configuration of screw superpartials before cross-slip. (b) Configuration of screw superpartials after cross-slip.

shown in Figure 1b. The PPV model indicates that the driving force of the cross-slip originates from the APB energy anisotropy, therefore, the activation enthalpy of cross-slip and the anomalous flow behavior of Ni_3Al largely depend on the APB, CSF energy on the (111) plane and the APB energy on the (001) plane.

Previous experiments have reported [7,9,10] that the planar fault energies are sensitive to the chemical compositions of Ni_3Al. Both experimental and theoretical results indicate that elements such as Re, Ru, Ta, Ti, and W have site preference for the Al sublattice in the γ' phase of superalloys [11–14]. How these alloying elements alter the planar fault energies and the activation enthalpy of cross-slip is not clear. The abilities of these alloying elements to increase flow stress and strengthening of Ni_3Al need to be evaluated, which is fundamental and essential for alloy design.

In this paper, the influences of Re, Ru, Ta, Ti, and W on dislocation cross-slip in γ'-Ni_3Al are explored in a combination of first-principles calculation and the theory of dislocation. The planar fault energies in Ni_3Al are chosen as the coupling physical parameters which bridge the electronic structure and the mechanical properties of the material. First-principles calculation results are used as the input parameters for analytical expressions based on classical dislocation theory to evaluate the effects of alloying elements on the activation enthalpy of dislocation cross-slip and the flow stress in the anomalous temperature regime of Ni_3Al.

The paper is organized as follows. Following the Introduction, Section 2 describes the computational method, the model and the results for the influences of alloying elements on the planar fault energies, including the analyses of electronic structures. The calculational details of the cross-slip activation enthalpy and the effects of alloying elements are presented in Section 3. Finally, a short summary is given in Section 4.

2. The influences of alloying elements on planar fault energies

2.1. *Computational method*

The density functional theory calculations were carried out with the plane-wave based Vienna *Ab Initio* Simulation Package [15,16] using the projector augmented wave method [17,18] and the spin-polarized generalized gradient approximation in the parametrization by Perdew *et al*. [19]. Plane waves have been included up to

a cutoff energy of 350 eV which yields converged results. The convergence accuracy of the total energy was chosen as 10^{-5} eV in the relaxation of the electronic degrees of freedom. The structures of the models were relaxed until the maximum force was less than 0.02 eV/Å. The scheme of k-point sampling was according to the Monkhorst–Pack scheme [20].

2.2. *Computational model*

For the calculation of planar fault energies, supercells were used by introducing a displacement on the (111) and (001) planes. Ni_3Al is a close-packed structure with an arrangement of three successive planes along the ⟨111⟩ direction as shown in Figure 2a. An APB or a CSF on the (111) plane was formed by shearing $a/2\langle\bar{1}01\rangle(111)$ or $a/6\langle\bar{1}\,\bar{1}2\rangle(111)$, respectively. An APB on the (001) plane was formed by shearing $a/2\langle110\rangle(001)$ in Figure 2b. A vacuum region of 12 Å was introduced to eliminate the interactions of parallel faults and the atoms in the top and bottom layers are fixed during relaxation to avoid surface reconfiguration.

2.3. *Calculational results and discussions*

The planar fault energy per unit area is defined as

$$\gamma_p = \frac{E_{fault} - E_{perfect}}{\Delta S} \tag{1}$$

where E_{fault} and $E_{perfect}$ are the total energies of the systems with and without the planar fault, respectively, and ΔS is the area of the planar fault region. The APB and CSF energies on the (111) plane are calculated in 6, 9, 12, 15, and 18 layers supercells (each layer containing eight atoms). The calculation results are shown in Figure 3a. From the results, it can be seen that the APB and CSF energies become convergent

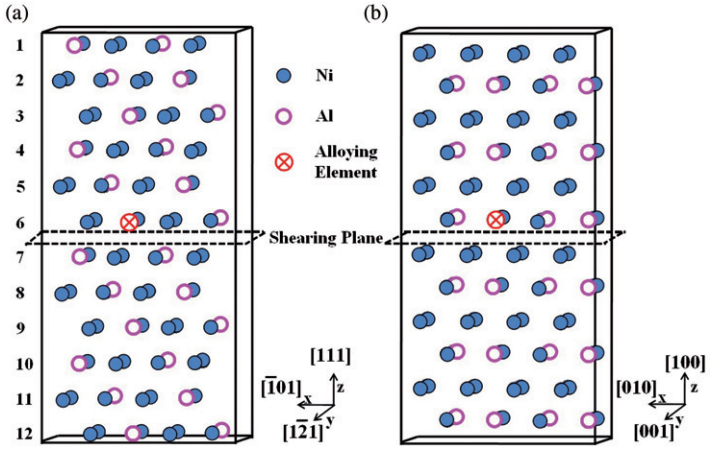

Figure 2. The calculational models. (a) Unsheared supercell along [111]. (b) Unsheared supercell along [100]. The blue full circle stands for the Ni atom. The pink open circle stands for the Al atom. The circle with a cross inside stands for the alloying atom.

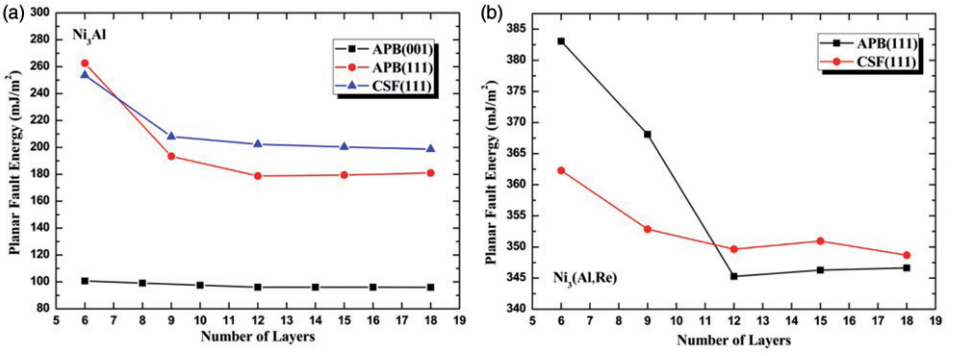

Figure 3. (a) Three kinds of planar fault energy in pure Ni_3Al for various system sizes. (b) The effects of Re on the APB and CSF energies on the (111) plane for various system sizes.

beyond 12 layers, hence a minimum supercell of 12 layers is required in order to eliminate the interaction between the fixed surface and the fault. The APB energy on the (001) plane is calculated in 6, 8, 10, 12, 14, 16, and 18 layers supercells (each layer containing eight atoms). The values in Figure 3a become nearly independent beyond 12 layers.

The planar fault energy per unit area with the alloying elements locating in the fault region is defined as

$$\gamma'_{\mathrm{p}}(i) = \frac{E^{\mathrm{b}}_{\mathrm{p}}(i) - E^{\mathrm{a}}_{\mathrm{p}}(i)}{\Delta S} \tag{2}$$

where $E^{\mathrm{b}}_{\mathrm{p}}(i)$ is the energy of the planar fault system with the alloying element i located in the planar fault region. $E^{\mathrm{a}}_{\mathrm{p}}(i)$ is the energy of the system without planar energy while the alloying element i substitutes for one Al atom. We take the element Re for example and calculate the effects of Re on the APB and CSF energies on the (111) plane in 6, 9, 12, 15, and 18 layers supercells (each layer containing eight atoms, one Re atom substitutes for an Al atom in the shearing plane) as shown in Figure 3b. The results show that beyond 12 layers, the changes of the APB and CSF energies in the $Ni_3(Al, Re)$ system are within 1%. These energy changes do not affect the relative comparisons between the effects of various alloying elements on fault energies, thus the effect of the imposed constraint (holding the surface atoms fixed) on the results can be negligible in the 12-layer models. Therefore, considering the convergence and the time consumption of the calculated models, we use the 12-layer models in our research. As a benchmark, the calculated planar fault energies of pure Ni_3Al per unit area are listed in Table 1, which agree well with the available experimental results.

The change in magnitude of fault energies for a given alloying element is a function of its distance from the planar fault. We calculate the effects of alloying elements on the APB and CSF energies on the (111) plane in 12-layer supercells as the distance between the element and the planar fault increases. As shown in Figure 2a, one alloying element substitutes for an Al atom in layers 6, 5, and 4, respectively. The results in Figure 4a and b show that the effects of alloying elements on the fault energies decrease rapidly as the distance between the element and the

Table 1. The planar fault energies in pure γ'-Ni_3Al.

Fault energy		Experimental results			First-principles calculations: Present work	First-principles calculations: Others	
APB	γ^{111}_{APB} (mJ/m^2)	175[a]	195[b]	180[c]	178.76	188[d]	175[e]
	γ^{001}_{APB} (mJ/m^2)	104[a]	160[b]		96.05	115[d]	140[e]
CSF	γ_{CSF} (mJ/m^2)	235[a]	236[b]	206[c]	202.32	319[d]	225[e]

Notes: [a]Ref. [7].
[b]Ref. [21].
[c]Ref. [22].
[d]Ref. [23].
[e]Ref. [24].

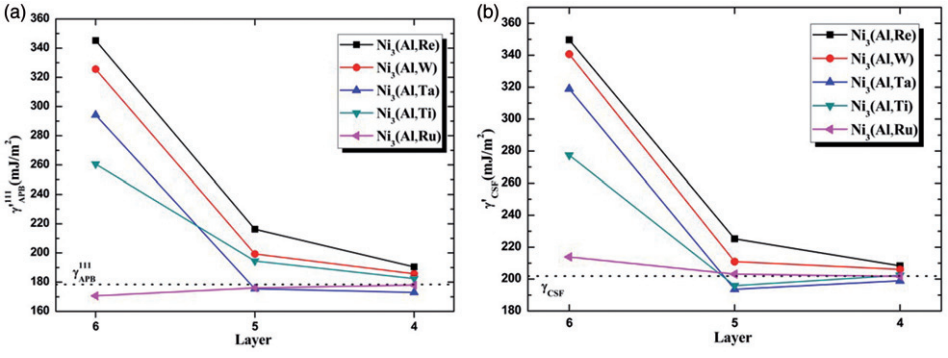

Figure 4. (a) The APB (111) energies in various alloying systems with different distances between the element and the fault plane. γ^{111}_{APB} in the figure is the APB energy in pure Ni_3Al. (b) The CSF energies in various alloying systems with different distances between the element and the fault plane. γ_{CSF} in the figure is the CSF energy in pure Ni_3Al.

fault region increases. When the alloying element substituting for an Al atom is in layer 4, the values of the planar fault energies in various alloying systems are close to the values in pure Ni_3Al, which means the interaction between the alloying element and the fault is a local effect. For the comparison of the effects on planar fault energies between different alloying elements, we use the values of fault energies when the alloying elements are in the fault planes.

The effects of alloying elements on three kinds of planar fault energies are summarized in Table 2. It can be concluded that under the same concentrations, all the elements raise the APB energies on (001) planes. On (111) planes, Re, W, and Ta increase the APB and CSF energies remarkably, and Ti can also increase the planar fault energies to some extent; however, Ru decreases the APB and slightly increases the CSF energies.

To gain a deeper insight into the origin of these effects, the electronic charge density differences in the APB and CSF region are plotted, as presented in Figure 5. As seen from the figures, more electrons are accumulated between Re, W, and Ta

Table 2. The influence of alloying elements on three kinds of planar fault energies.

Alloy system	γ'^{001}_{APB} (mJ/m^2)	γ'^{111}_{APB} (mJ/m^2)	γ'_{CSF} (mJ/m^2)	$\Delta\gamma^{001}_{APB}$ (mJ/m^2)	$\Delta\gamma^{111}_{APB}$ (mJ/m^2)	$\Delta\gamma_{CSF}$ (mJ/m^2)
Ni_3Al(Re)	99.41	345.27	349.64	3.36	166.51	147.32
Ni_3Al(Ru)	109.68	170.62	213.31	13.63	−8.14	10.99
Ni_3Al(Ta)	155.42	294.15	318.97	59.37	115.39	116.65
Ni_3Al(Ti)	140.31	260.63	277.46	44.26	81.87	75.14
Ni_3Al(W)	166.63	325.57	340.65	70.58	146.81	138.33

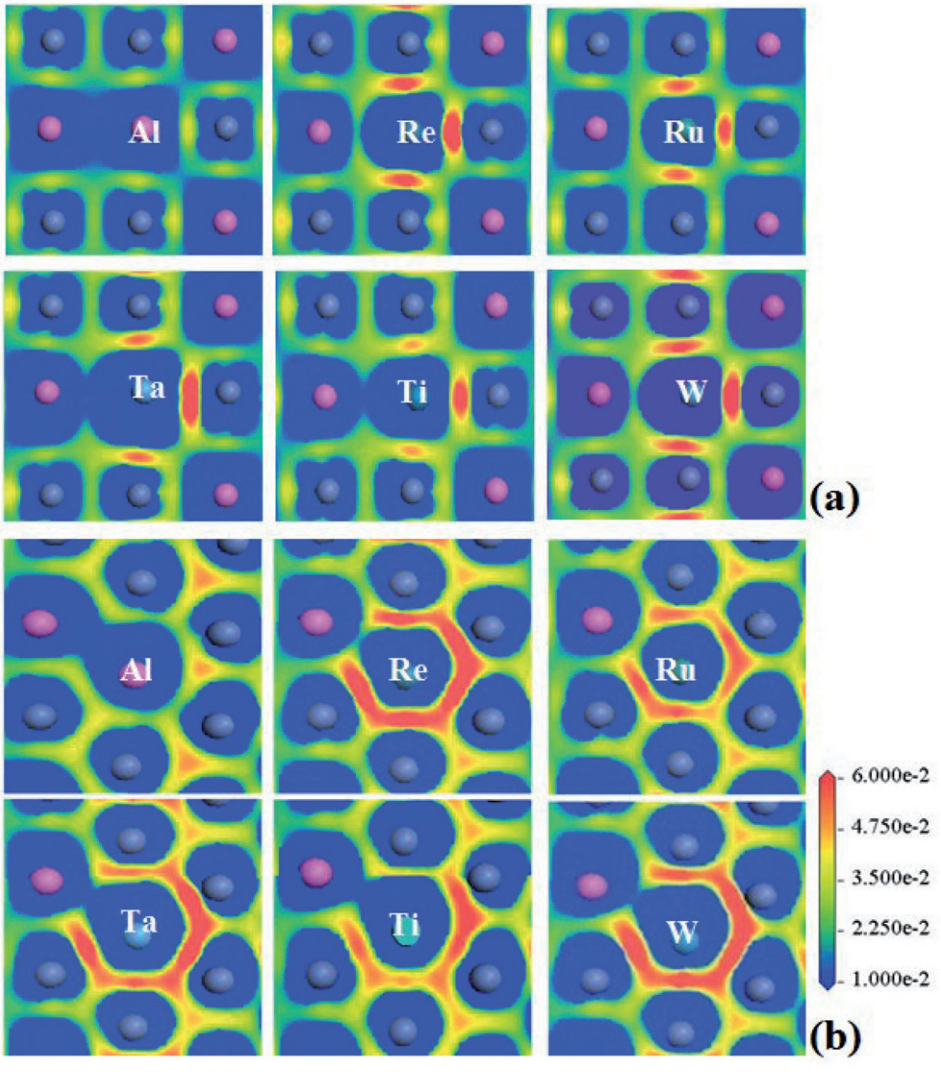

Figure 5. The electronic charge density differences in (a) the APB region and (b) the CSF region with the Al atom or alloying elements in the center.

and their first-nearest-neighbor (FNN) Ni atoms. Besides, obvious accumulations of electrons between Ru and its FNN Al atom are found. These indicate that the bonds of Re–Ni, W–Ni, and Ta–Ni are stronger than those of Ru–Ni and Ti–Ni; however, the Ru–Al bonding is strongest. Because of the $L1_2$ structure, every Al site is surrounded by 12 FNN Ni atoms in perfect Ni_3Al. After forming the APB and CSF on the (111) plane, the FNN atoms of the Al site in the fault region become 11 Ni atoms and 1 Al atom. The process of forming the APB or CSF involves the breaking of the bonds between the alloying elements and their FNN Ni atoms and formation of the bonds between alloying elements and their FNN Al atoms. Therefore, the breaking of Re–Ni, W–Ni, and Ta–Ni bonds will need more energy and they can increase the planar fault energies more remarkable. On the other hand, the low planar fault energies in Ni_3Al(Ru) may be attributed to the strongest bonding of Ru–Al. As discussed in our previous work, there exist d-d hybridizations between Re–Ni, W–Ni, and Ta–Ni, which result in strong bondings [25–27]. The understanding of strong bonding of Ru–Al can be helped by comparing the partial density of states of Al atoms as presented in Figures 6 and 7. In Figure 6, the solid lines represent the p electron DOS of the FNN Al atoms of Al and alloying elements in the fault regions, and the dotted line represents the p electron DOS of Al in perfect Ni_3Al. Compared to the Al atom in perfect Ni_3Al, there is very evident splitting of the p band into bonding and antibonding states near the Fermi level E_F for the FNN

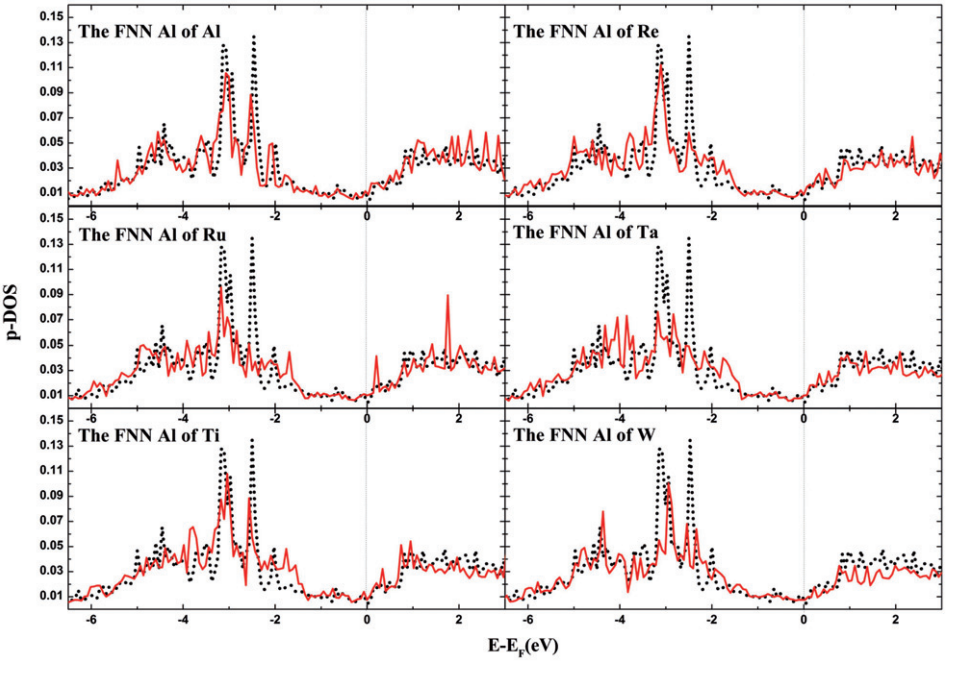

Figure 6. The p electron DOS (p-DOS) of Al atoms: the solid lines represents the p-DOS of the FNN Al atoms of Al and alloying elements in fault regions; the dotted lines represent the p-DOS of Al in perfect Ni_3Al. The Fermi level is shifted to zero.

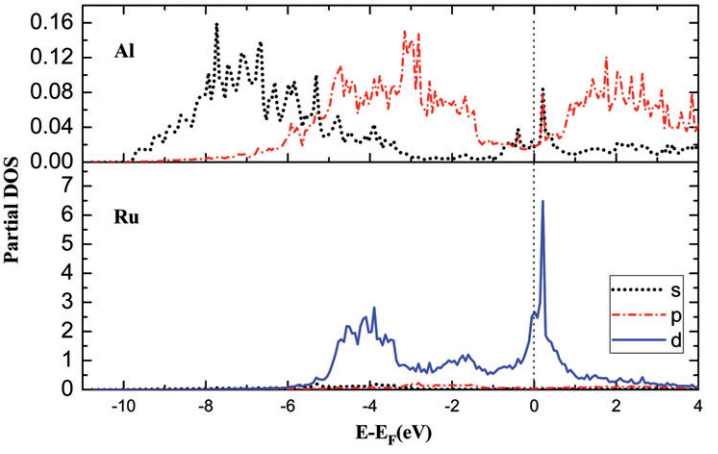

Figure 7. The partial DOS of Ru and its FNN Al atom. Dotted, dash-dot and solid lines stand for s, p, d electrons, respectively. The Fermi level is shifted to zero.

Al of Ru. This suggests the formation of localized states between Ru and Al which originates from p-d orbit hybridization as shown in Figure 7. Some p electrons of Al are transferred to deeper energy levels to participate in the bonding with the d electrons of Ru. In contrast, the splitting is not so obvious on the DOS for other alloying elements.

3. The influences of alloying elements on activation enthalpies of dislocation cross-slip

Based on the PPV model [5–7], the activation enthalpy needed for a screw dislocation cross-slipping from the (111) to the (001) plane can be given as follows:

$$H_C = 2E_C + b\left[\frac{\mu b^2}{8\pi} - \left(\frac{\mu b^3}{8\pi}F\right)^{1/2}\right] \tag{3}$$

$$F = \sqrt{3}\gamma_{\mathrm{APB}}^{111}\frac{A}{A+2} - \gamma_{\mathrm{APB}}^{001} \tag{4}$$

$$A = 2\frac{C_{44}}{(C_{11}-C_{12})} \tag{5}$$

where μ is the shear modulus, b is the length of the Burgers vector, F is the force per unit length of dislocation which promotes cross-slip, A is the Zener anisotropy ratio, C_{11}, C_{44}, and C_{12} are the elastic constants, and the energy of one constriction E_c can be obtained by Sorth's method [28,29]:

$$E_c = 2\left[\frac{\mu\vec{b_1}\cdot\vec{b_2}}{2\pi}T_1\right]^{1/2} D_C I(C) \tag{6}$$

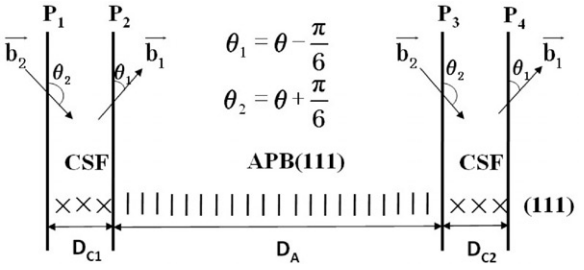

Figure 8. Diagrammatic drawing of the dissociation of a superlattice dislocation into four partials.

where D_C is the equilibrium width of the CSF region, as shown in Figure 8, θ is the angle between the dislocation line and the Burgers vector $a/2\langle\bar{1}01\rangle$, T_1 is the line tension and $I(C) = 0.55C$ is the integrating parameter, where

$$C = \cos(\theta + \pi/6)\cos(\theta - \pi/6) + \sin(\theta + \pi/6)\sin(\theta - \pi/6)/(1 - \nu), \tag{7}$$

ν is Poisson's ratio, and $\overrightarrow{b_1}$ and $\overrightarrow{b_2}$ are the Burgers vectors of two Shockley partial dislocations.

In order to obtain D_{C1} and D_{C2} in Figure 8, the equilibrium equations of forces acting on each partial are listed as follows:

*P*1:

$$\gamma_{CSF} = \frac{f_{21}}{D_{C1} + D_A + D_{C2}} + \frac{f_{22}}{D_{C1} + D_A} + \frac{f_{21}}{D_{C1}} \tag{8}$$

*P*2:

$$\gamma_{CSF} - \gamma_{APB}^{111} = -\frac{f_{11}}{D_A + D_{C2}} - \frac{f_{12}}{D_A} + \frac{f_{12}}{D_{C1}} \tag{9}$$

*P*3:

$$-\gamma_{CSF} + \gamma_{APB}^{111} = -\frac{f_{21}}{D_{C2}} + \frac{f_{21}}{D_A} + \frac{f_{22}}{D_{C1} + D_A} \tag{10}$$

*P*4:

$$\gamma_{CSF} = \frac{f_{12}}{D_{C2}} + \frac{f_{11}}{D_A + D_{C2}} + \frac{f_{12}}{D_{C1} + D_A + D_{C2}} \tag{11}$$

where

$$f_{ij} = \frac{\mu}{2\pi}\left[(\overrightarrow{b_i}\cdot\overrightarrow{\zeta_i})(\overrightarrow{b_j}\cdot\overrightarrow{\zeta_j}) + \frac{(\overrightarrow{b_i}\times\overrightarrow{\zeta_i})(\overrightarrow{b_j}\times\overrightarrow{\zeta_j})}{1-\upsilon}\right](i = 1, 2; j = 1, 2), \tag{12}$$

and $\overrightarrow{\zeta_1}$ and $\overrightarrow{\zeta_2}$ are dislocation line directions. By solving Equations (8–11), the numerical values of D_{C1}, D_{C2}, and D_A can be obtained, then the energy of

Table 3. The effects of alloying elements on D_{C1}, D_{C2}, D_A, F, E_c, and H_c in different alloy systems.

Alloy system	D_{C1} (nm)	D_A (nm)	D_{C2} (nm)	F (mJ/m^2)	E_c (eV)	H_c (eV)
Ni_3Al	0.876	3.601	0.876	96.30	0.35	0.89
Ni_3Al(Re)	0.861	3.834	0.396	275.42	0.09	0.31
Ni_3Al(Ru)	0.873	3.633	0.805	73.86	0.31	0.83
Ni_3Al(Ta)	0.862	3.808	0.448	161.01	0.12	0.41
Ni_3Al(Ti)	0.865	3.760	0.544	184.37	0.17	0.49
Ni_3Al(W)	0.861	3.827	0.410	183.59	0.10	0.36

constrictions can be calculated using Equation (6), therefore, the activation enthalpy of cross-slip H_c can be acquired by using Equations (3–5). As a benchmark, H_c in pure Ni_3Al was calculated and listed in Table 3, and the results of the present work in Table 1 were chosen as the values of γ_{APB}^{111}, γ_{CSF} and γ_{APB}^{001}; 78 GPa, 224.5 GPa, 124.4 GPa, 148.6 GPa, and 0.305 were chosen as the values of μ, C_{11}, C_{44}, C_{12} and ν from previous experimental results [30]. As discussed by Parthasarathy and Dimiduk [31], the experimental cross-slip activation enthalpy is in the range 0.5–0.9 eV. Our calculation result is 0.89 eV, which agrees well with experimental results.

We suppose that the Shockley partial dislocations P_3 and P_4 in Figure 8 are leading pairs and P_1 and P_2 are trailing pairs. The leading pairs firstly come across the alloying elements and begin to constrict and cross-slip to the (001) plane while the trailing pairs are still on the (111) plane. By using the data in Table 2, the effects of alloying elements on the activation enthalpy are shown in Table 3. The results show that the reductions of the cross-slip activation enthalpy due to alloying elements are in the order Re > W > Ta > Ti > Ru. The planar fault energies not only determine the driving forces of cross-slip to a great extent but also influence the widths of two CSF regions which have direct relationships with the energies of constrictions. Re, W, Ta, Ti, and Ru increase the CSF energies and decrease the width of the CSF region leading to lower constriction energies. Meanwhile, Re, W, Ta, and Ti also promote driving forces of cross-slip, hence the values of the activation enthalpy fall. The lower the activation enthalpy is, the more easily cross-slip may occur to form dislocation locks, thus leading to more difficult dislocation motion and higher flow stress in the anomalous temperature regime of Ni_3Al. All these effects originate from the changes of electronic structure caused by alloying elements in fault areas, as discussed in Section 2. Thus, the relationship between the electronic structures of alloying element–planar fault complex and the dislocation cross-slip activation enthalpy has been built. This relationship has been confirmed by compression tests and transmission electron microscopy experiments in the Ni_3Al (1at.% Ta) ternary system [7,32,33]. Compared to the Ni_3Al binary alloy, Ta was found to increase the APB and CSF energies on the (111) plane and raise the flow stress in the anomalous regime. From our calculation results, Re and W can be predicted to be more efficient in strengthening Ni_3Al than Ta.

4. Summary

First-principles electronic structure calculations combined with classical dislocation theory are used to study the influences of alloying elements on the planar fault energies and the dislocation cross-slip activation enthalpy.

Re, W, and Ta are found to increase the APB and CSF energies on the (111) plane remarkably. Ti also raises both of the planar fault energies to some extent. Ru decreases the APB and slightly increases the CSF energies on (111). The strong bonding of Re, W, and Ta with their surrounding Ni atoms and weak bonding with their FNN Al atoms in fault areas are the reason that they increase the APB and CSF energies more than other elements. The strong bond due to d–p orbit hybridization between Ru and its FNN Al atom induces the lowest fault energies. Using the procedures mentioned in Section 3, the evaluation of the strengthening effects of various alloying elements can be given. The abilities of alloying elements to decrease the cross-slip activation enthalpy are in the order Re > W > Ta > Ti > Ru. Re and W are predicted to be more effective than Ta, Ti, and Ru in increasing the flow stress and strengthening γ'-Ni_3Al.

Acknowledgments

This work is supported by the National Basic Research Program ('973' Project, Ministry of Science and Technology of China, Grant No. 2011CB606402) and the National Natural Science Foundation (Ministry of Science and Technology of China, Grant No. 51071091).

References

[1] R.C. Reed, *Superalloys: Fundamentals and Applications*, Cambridge University Press, Cambridge, 2006.
[2] T.M. Pollock and A.S. Argon, Acta Metall. Mater. 40 (1992) p.1.
[3] T.M. Pollock and S.J. Tin, Propul. Power 22 (2006) p.361.
[4] B.H. Kear and H.G.F. Wilsdorf, Trans. AIME 224 (1962) p.382.
[5] V. Paidar, D.P. Pope and V. Vitek, Acta Metall. 32 (1984) p.435.
[6] M.H. Yoo, Scripta Metall. 20 (1986) p.915.
[7] H.P. Karnthaler, E.T.H. Muhlbacher and C. Rentenberger, Acta Mater. 44 (1996) p.547.
[8] A.H.W. Ngan, M. Wen and C.H. Woo, Com. Mat. Sci. 29 (2004) p.259.
[9] D.M. Dimiduk, A.W. Thompson and J.C. Williams, Phil. Mag. A 67 (1993) p.675.
[10] N. Baluc, H.P. Karnthaler and M.J. Mills, Phil. Mag. A 64 (1991) p.137.
[11] A.V. Ruban and H.L. Skriver, Phys. Rev. B 55 (1997) p.856.
[12] C. Jiang and B. Gleeson, Scripta Mater. 55 (2006) p.433.
[13] Y. Zhou, Z. Mao, B.M. Christopher and D.N. Seidman, Appl. Phys. Lett. 93 (2008) p.171905.
[14] Y. Amouyal, Z. Mao, B.M. Christopher and D.N. Seidman, Appl. Phys. Lett. 94 (2009) p.041917.
[15] G. Kresse and J. Hafner, Phys. Rev. B 47 (1993) p.558.
[16] G. Kresse and J. Furthmuller, Phys. Rev. B 54 (1996) p.11169.
[17] P.E. Blochl, Phys. Rev. B 50 (1994) p.17953.
[18] G. Kresse and D. Joubert, Phys. Rev. B 59 (1999) p.1758.
[19] J.P. Perdew, K. Burke and M. Ernzerhof, Phys. Rev. Lett. 77 (1996) p.3865.
[20] H.J. Monkhorst and J.D. Pack, Phys. Rev. B 13 (1976) p.5188.

[21] T. Kruml, E. Conforto, B.L. Piccolo, D. Caillard and J.L. Martin, Acta Mater. 50 (2002) p.5091.
[22] H. Hemker and M.J. Mills, Phil. Mag. A 68 (1993) p.305.
[23] A.T. Paxton and Y.Q. Sun, Phil. Mag. A 78 (1998) p.85.
[24] C.L. Fu, Y.Y. Ye and M.H. Yoo, Proc. MRS fall meeting: Symposium L 288 (1992) p.21.
[25] Y.J. Wang and C.Y. Wang, Phil. Mag. 89 (2009) p.2935.
[26] Y.J. Wang and C.Y. Wang, Proc. MRS fall meeting: Symposium FF 1224 (2009) p.1224-FF05-31.
[27] X.X. Yu and C.Y. Wang, Acta Mater. 57 (2009) p.5914.
[28] A.N. Stroh, Proc. Phys. Soc. London, Sec. B 67 (1954) p.427.
[29] C.Y. Wang, S.Y. Liu and L.G. Han, Phys. Rev. B 41 (1990) p.1359.
[30] S.V. Prikhodko, J.D. Carnes, D.G. Isaak, H. Yang and A.J. Ardell, Metall. Mater. Trans. A 30 (1999) p.2043.
[31] T.A. Parthasarathy and D.M. Dimiduk, Acta Mater. 44 (1996) p.2237.
[32] M.A. Crimp and P.M. Hazzledine, Mat. Res. Soc. Symp. Proc. 133 (1989) p.131.
[33] M.J. Mills, N. Baluc and H.P. Karnthaler, Mat. Res. Soc. Symp. Proc. 133 (1989) p.203.